ARTICLES

Journal of Semiconductors
(2019) 40, 052101
doi: 10.1088/1674-4926/40/5/052101

Structural and optical studies on PVA capped SnS films grown by chemical bath deposition for solar cell application

P Mallika Bramaramba Devi, G. Phaneendra Reddy, and K. T. Ramakrishna Reddy†

Solar Energy Laboratory, Department of Physics, Sri Venkateswara University, Tirupati-517502, India

Abstract: Tin monosulphide (SnS) thin films capped by PVA have been successfully deposited on glass substrates for cost effective photovoltaic device applications by a simple and low-cost wet chemical process, chemical bath deposition (CBD) at different bath temperatures varying in the range, 50–80 °C. X–ray diffraction analysis showed that the deposited films were polycrystalline in nature, showing orthorhombic structure with an intense peak corresponding to (040) plane of SnS. These observations were further confirmed by Raman analysis. FTIR spectra showed the absorption bands which corresponds to PVA in addition to SnS. The scanning electron microscopy and atomic force microscopy studies revealed that the deposited SnS films were uniform and nanostructured with an average particle size of 4.9 to 7.6 nm. The optical investigations showed that the layers were highly absorbing with the optical absorption coefficient ~10^5 cm^{-1}. A decrease in optical band gap from 1.92 to 1.55 eV with an increase of bath temperature was observed. The observed band gap values were higher than the bulk value of 1.3 eV, which might be due to quantum confinement effect. The optical band gap values were also used to calculate particle size and the results are discussed.

Key words: chemical bath deposition; polyvinyl alcohol; capping agent; SnS thin films; structural properties; optical properties

Citation: P M B Devi, G P Reddy, and K T R Reddy, Structural and optical studies on PVA capped SnS films grown by chemical bath deposition for solar cell application[J]. *J. Semicond.*, 2019, 40(5), 052101. http://doi.org/10.1088/1674-4926/40/5/052101

1. Introduction

Recent investigations on photovoltaic devices emphasize the importance of semiconducting metal chalcogenide thin film solar cells at low cost. The IV–VI group semiconductors are highly attractive for their novel properties suitable for optoelectronic applications and can be synthesized by using simple techniques in thin film form. Tin monosulphide (SnS) belongs to this group of materials that has three stable binary phases, SnS, SnS_2 (both layer structures) and Sn_2S_3 (ribbon structure)[1]. Tin monosulphide (SnS) has a direct optical band gap of 1.3 eV[2], which is close to the optimum value of 1.5 eV and also an indirect band gap of 1.09 eV. Further, SnS attracts the attention of many researchers because of the natural abundance of its constituent elements, low toxicity, low cost, and direct energy band gap with high optical absorption coefficient (> 10^4 cm^{-1}) and high hole mobility (~ 90 $cm^2V^{-1}s^{-1}$)[3–6]. Hence SnS is a potential candidate as an absorber layer in photovoltaic devices[7, 8]. Various physical and chemical methods are used to deposit SnS layers on glass substrates. These include spray pyrolysis[9], thermal evaporation[10], electron beam evaporation[11], magnetron sputtering[12] and liquid-phase deposition[13]. As physical methods involve complicated instrumentation and are highly expensive; therefore, chemical methods are preferable. In terms of experimental requirements, chemical bath deposition is a very simple technique that offers low processing temperature, easy composition control, good homogeneity and therefore has physical significance in the production of large area devices at low cost[14, 15]. Therefore, in the present study, we have chosen chemical bath deposition technique to grow SnS nanocrystals. Excessive research reports are available in literature on the deposition of SnS films using CBD at different deposition conditions[16–20] and also the effect of various dopants added to SnS films using CBD[21–24].

It is known that due to high surface to volume ratio and quantum size effects, the nanostructured materials offer great advantages than the bulk materials. Various reports are available on synthesis of SnS nanoparticles using different techniques[25–28]. Using SnS nanoparticles, different researchers fabricated solar cells, which showed efficiencies upto 0.5%[29]. Capping is a prominent method to achieve better surface states of the nanoparticles. Capping provides surface passivation, which leads to a change in the surface states and reduction in the crystallite size[30, 31]. Polymer capped thin films have greater stability than uncapped films. Polymer capped semiconductor layers had enhanced and tunable optical, and electrical properties for their potential applications in various fields such as solar cells, field effect transistors, optical switching, light emitting diodes and photodetectors[32–35]. Many materials such as polyvinyl alcohol, polyacrylic acid, polyacrylonitrile, polyethylene glycol, polymethyl methacrylate and polyvinylpyrrolidone have been used as capping agents[36, 37]. Among all these polymers, there is currently a great interest in polyvinyl alcohol (PVA) for researchers due to its superior properties such as good film forming ability, bio-degradability, non-toxicity, hydrophilicity, low cost, chemical resistance and transparency over the whole visible spectrum[38–40]. PVA stabilizes the SnS nanocrystals preventing them from coagulation, but do not alter the intrinsic characteristics of SnS.

Few works on synthesis of various semiconducting nanostructures capped by PVA are reported[41–43]. Simultaneously few reports are available in literature of solar cells fabricating using different semiconductors capped by PVA. Neetu *et al.*[44] fabricated ZnO based quantum dot sensitised solar cell via chemical route using CdS quantum dots capped by PVA

Correspondence to: K T R Reddy, ktrkreddy@gmail.com
Received 22 JANUARY 2019; Revised 30 MARCH 2019.

Table 1. Data of the SnS thin films deposited on glass substrates at different deposition temperatures reported in literature.

Deposition method	Deposition temperature (°C)	Phase	Sn/S ratio	α (cm^{-1})	Band gap (eV)	Ref.
CBD (uncapped)	40–80	SnS	–	10^4	1.41–1.30	[47]
Sulfurization	150–450	SnS (300–350 °C), SnS + Sn_2S_3 (150–200 °C), SnS + SnS_2 (400–450 °C)	–	–	1.2–1.6	[48]
Thermal evaporation	200–400	SnS	0.96-1.10	–	1.36	[49]
RF sputtering	150–300	SnS	–	–	1.67–1.44	[50]
MOCVD	430–470	SnS	0.92–1.32	10^4	1.3–1.1	[51]
Spray pyrolysis	250–450	SnS (250–400 °C), SnS + Sn_2S_3 (450 °C)	1.29–1.11	–	1.70–1.46	[52]
Electron beam evaporation	300	SnS	–	–	1.38	[11]
CVD	200–400	SnS	2.77–1.15	–	–	[53]
Spin coating	150–400	SnS (200 °C), SnS + SnS_2 (300 °C), SnS + Sn_2S_3 (400 °C)	1.31–1.03	–	1.88–1.26	[54]
CBD (PVA capping)	50–80	SnS (70–80 °C), SnS + Sn_2S_3 + SnS_2 (70–80 °C)	0.46–0.95	10^5	1.92–1.55	Present work

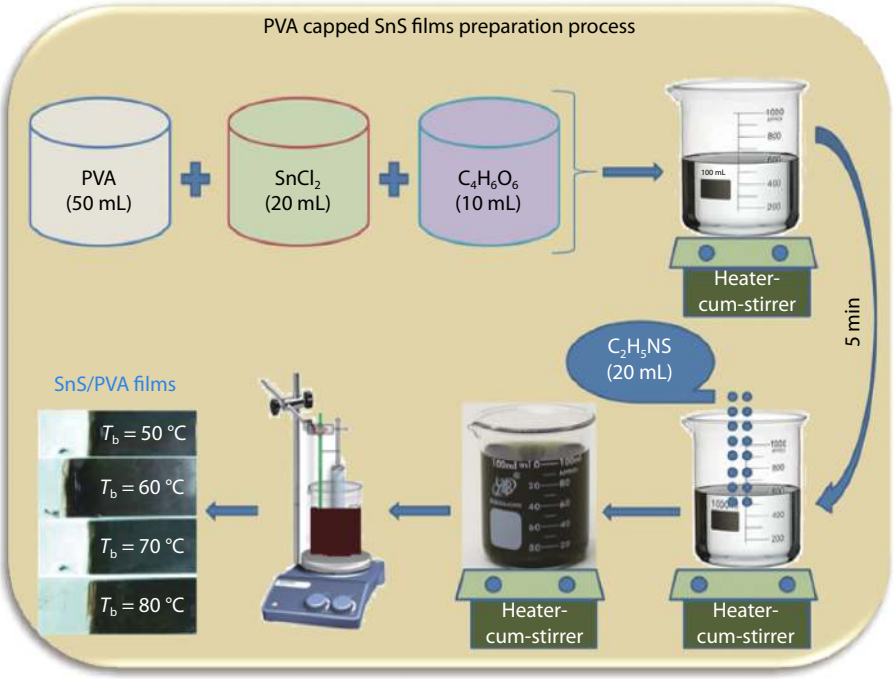

Fig. 1. (Color online) Schematic diagram of preparation of PVA capped SnS films.

showed 1.3% efficiency. Phukan *et al.*[45] synthesized CdSe quantum dots dispersed in PVA matrix using heat induced thermolysis technique as a window layer and the cell showed an efficiency of 2.43%. Recently, solar cells fabricated using chemical bath deposition technique with PbS capped by PVA as an absorber layer and CdS capped by PVA as a window layer by Saikia *et al.*[46] showed an efficiency of 1.67% under 1 Sun illumination. From these investigations, it is evident that PVA capping agent had been effectively used in photovoltaic devices and attention of further development on these economical photovoltaic devices in both material and cost wise reduction had been encouraged in research studies. To the best of our knowledge, there is no previous literature reported on PVA capped SnS thin films deposited by chemical bath deposition. Table 1 shows the reported literature[11, 47–54] on SnS thin films deposited using different methods. A critical analysis of the literature indicated that deposition of SnS films in all the methods, except CBD was carried out at high temperatures. Further, the optical absorption coefficient reported for SnS films formed by MOCVD and CBD (uncapped SnS layers) methods is of the order 10^4 cm^{-1}. A higher optical absorption coefficient for the films is highly desirable to use such films as an absorber layer in a solar cell to maximize the absorption of solar radiation. Further, deposition of thin films at lower growth temperatures is very crucial in the cradle-to-grave life cycle cost analysis of any device developed using thin films, particularly in the case of a solar cell. Therefore in the present work, PVA capped SnS layers were grown using the simple CBD process and a detailed investigation of structural and optical properties were made with the aim to improve the optical behaviour of the grown layers. The effect of varying bath temperature on these properties was analyzed and reported.

2. Experimental details

2.1. Chemicals

In the present study, stannous chloride ($SnCl_2$, $2H_2O$) was used as the source material for tin and thioacetamide (C_2H_5NS) for sulphur. Tartaric acid ($C_4H_6O_6$) was used as a complexing

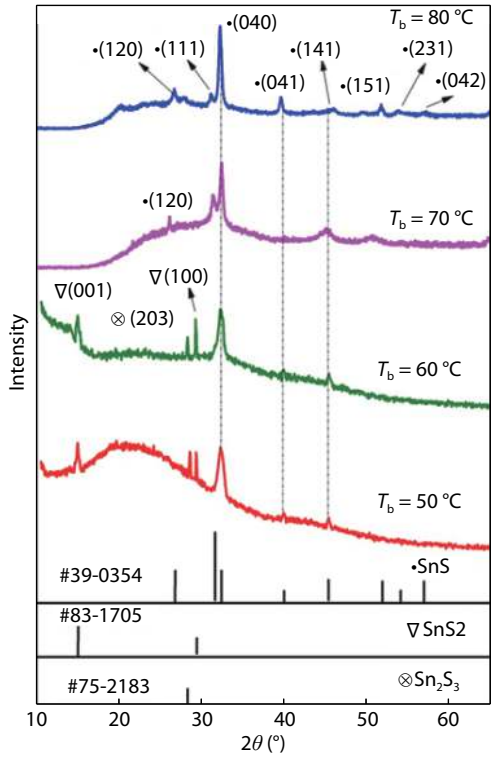

Fig. 2. (Color online) X-ray diffraction patterns of SnS films grown at different bath temperatures.

agent and polyvinyl alcohol $(–CH_2CHOH–)_n$ (average M.W. = 1 60 000) as capping agent to prepare SnS thin films.

2.2. Method

The PVA capped SnS thin films were prepared using chemical bath deposition as shown in Fig. 1. Initially, 2 g of PVA was dissolved in 100 mL water, contained in a beaker and stirred at 80 °C by using a magnetic stirrer, which has a facility to control the temperature until a viscous transparent solution was obtained and then allowed to cool to the room temperature. Fresh solutions of 0.1 M stannous chloride ($SnCl_2$, $2H_2O$), 0.2 M thioacetamide (C_2H_5NS) and 0.5 M tartaric acid were prepared using double distilled water such that the precursor ratio of S/Sn was maintained as 2. Initially, 20 mL of stannous chloride and 10 mL of tartaric acid were added to 50 mL of previously prepared PVA solution in a glass beaker and stirred well by a magnetic stirrer at a rate of 200 revolutions per minute. After 5 min, 20 mL of thioacetamide was added to the solution Lsuch that the total volume of the solution becomes 100 mL. Now, cleaned glass substrates were immersed vertically into the solution to deposit SnS films. The deposition of SnS films were carried out for a fixed time of 90 min at different bath temperatures that varied from 50 to 80 °C. The deposited films were cleaned using distilled water and dried in a hot air oven. The visual observation of the deposited layers indicated dark brown colour and the films were well adherent to the glass substrate surface without any visible pinholes and cracks.

The deposited SnS layers were characterized using appropriate techniques. The X-ray diffraction patterns of the layers deposited on glass substrates at different bath temperatures were recorded using Burker (D8 Advance) X-ray diffractometer, using CuKα (λ = 1.5408 Å) radiation at room temperature. The Raman spectra were recorded in the backscattering configuration at room temperature with unpolarized light using DI-POLAR XY 800 Raman spectrometer. FTIR absorption spectra for the deposited experimental films were recorded using Thermo Nicolet FTIR spectrophotometer. The morphology of the layers was observed by using a Carl Zeiss EVO 50 scanning electron microscope (SEM). Solver Nano NT-MDT atomic force microscope (AFM) was used to investigate the surface roughness of the films. The optical transmittance measurements were carried out using JASCO V-770 UV-VIS-NIR spectrophotometer, using unpolarized light.

3. Results and discussions

3.1. Structural analysis

3.1.1. X-ray diffraction studies

X-ray diffraction analysis was undertaken to investigate the structural properties of the deposited SnS layers. Fig. 2 shows the typical X-ray diffraction patterns of SnS films capped by PVA at different temperatures that varied in the range of 50–80 °C. The XRD spectrum indicated many peaks in all the deposited films with an intense (040) peak observed at $2\theta = 32.0°$. In addition, all the observed peaks were broad, indicating nanocrystalline nature of the grown layers. The films deposited at bath temperatures < 70 °C exhibited secondary phases such as Sn_2S_3 and SnS_2 in addition to SnS. The peaks observed at $2\theta = 15.02°$ and $2\theta = 28.39°$ corresponds to (001) and (100) planes of SnS_2 and the peak at $2\theta = 27.73°$ corresponds to (203) plane of Sn_2S_3 respectively that matches with the standard data reported in JCPDS card no. 83-1705 and 75-2183. Also the peaks observed at 2θ = 26.02°, 31.50°, 39.40° and 44.88°, 51.42° 53.89° 56.73° corresponds to (120), (111), (041), (141), (151), (231) and (042) planes of SnS phase with orthorhombic crystal structure as reported in JCPDS card no. 39-0354. Kalandragh *et al.*[28] also reported (040) as the preferred orientation for SnS nanocrystals produced by ultrasound-assisted method. The intensity of secondary phases decreased with the increase of bath temperature and finally they disappeared at higher bath temperatures ⩾ 70 °C. Thus the layers deposited at 70 and 80 °C exhibited only the planes corresponding to SnS phase. The intensity of (040) peak increases with increase of deposition temperature, which shows an improvement in crystallinity of SnS films with deposition temperature.

Various structural parameters such as the average crystallite size, dislocation density, strain and number of crystallites per unit area were evaluated using X-ray diffraction data. The interplanar spacing d_{hkl} was calculated using the Bragg's diffraction principle,

$$n\lambda = 2d\sin\theta, \tag{1}$$

where n is an integer, λ is the wavelength of X-rays (1.5408 Å) and θ is the Bragg's diffraction angle.

The average crystallite size (D) of the layers was calculated using Debye-Scherrer formula[55],

$$D = \frac{K\lambda}{\beta\cos\theta}, \tag{2}$$

where K is the shape factor, which is equal to 0.94 and β is the full width at half maximum of the predominant peak.

The calculated crystallite size varied with bath temperature in the range, 11–22 nm, indicating an increasing trend with bath temperature. From this, it can be understood that

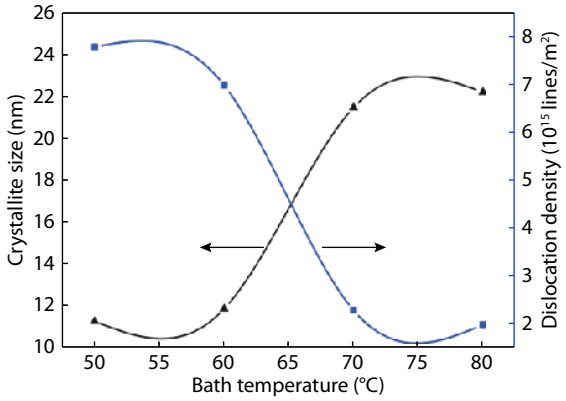

Fig. 3. (Color online) Change of crystallite size and dislocation density with bath temperature.

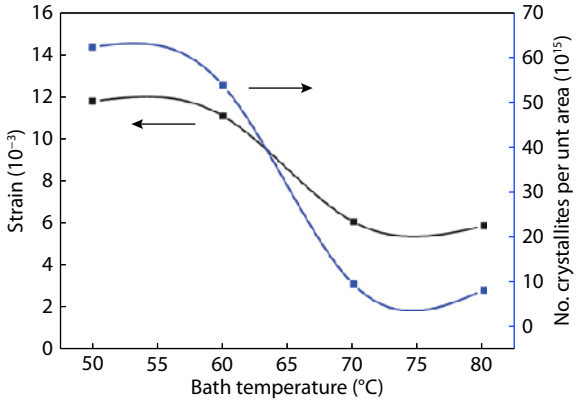

Fig. 4. (Color online) Variation of strain and number of crystallites per unit area of SnS layers with bath temperature.

with the increase of bath temperature, there will be an increase in kinetic energy of the reactants, which in turn increases the formation of nuclei on the surface of the substrate.

The dislocation density (δ) was determined using the following relation[56],

$$\delta = \frac{1}{D^2}, \tag{3}$$

Fig. 3 shows the change of crystallite size and dislocation density with bath temperature. It can be seen from the Fig. that values of δ varied in the range, 7.8×10^{15}–2.0×10^{15} m^{-2} with the increase of bath temperature from 50 to 80 °C. A minimum value of δ was observed for the layers grown at 80 °C due to improved crystallinity. This is because of the fact that the dislocations present at lower bath temperatures received more thermal energy at higher bath temperatures and hence moved from inside the crystallites to their grain boundaries and neutralized.

The lattice strain (ε) can be calculated by using the following relation[57],

$$\varepsilon = \frac{\beta}{4\tan\theta}, \tag{4}$$

where the symbols have usual meaning.

The evaluated strain values (shown in Fig. 4) decreased from 1.18×10^{-2} to 5.9×10^{-3} with the increase of bath temperature. This indicates that the strain in the layers deposited at lower bath temperature was higher due to the presence of crystal imperfections and dangling bonds. At higher temperatures there was a decrease in the lattice strain due to an increase in crystallite size and a decrease in dislocation density as the higher growth temperatures could annihilate the defects. The number of crystallites per unit area (N) was calculated using the relation[58],

$$N = \frac{t}{D^3}, \tag{5}$$

where t is the thickness of the films, ~ 90 nm as determined from SEM cross-section. Fig. 4 also shows the variation of number of crystallites with the increase of bath temperature. The number of crystallites per unit area varied between 6.2×10^{16} and 8.4×10^{15} with the raise of bath temperature from 50 to 80 °C. This is because of the fact that higher temperatures could provide higher thermal energy so that small crystallites coalesce together to form big ones, leading to the formation of large crystallites.

In XRD peaks, the observed broadening is considered to be due to the sum of contributions by the crystallite size and strain distribution present within the sample. Thus the crystallite size estimated from Scherrer's equations could be different from the actual crystallite size. Therefore, those contributions of size and strain must be separated by a more elaborated analysis, such as Williamson-Hall (W-H) plot. The average crystallite size and residual strain were described using the following equation[59]

$$\beta_{hkl}\cos\theta = \frac{k\lambda}{D} + 4\varepsilon\sin\theta. \tag{6}$$

Fig. 5 shows the W-H plots of the deposited SnS layers at bath temperatures varied from 50 to 80 °C. The intercept of the linear fit on the y-axis gives the average crystallite size and the slope of the linear fit gives the corresponding residual strain value. The estimated average crystallite size varied in the range, 4–11 nm and the strain values varied in the range, 2.24×10^{-2} to 6.9×10^{-3} nm with bath temperature were given in the Table 2. Thus the average crystallite size increases and the strain decreases with increase in bath temperature as was already discussed earlier. The calculated structural parameters of SnS films prepared via chemical bath deposition technique at different bath temperatures are listed in Table 2.

Further, Rietveld refinement analysis confirms the existence of orthorhombic SnS phase present in the deposited films. Fig. 6 shows the Rietveld refinement of deposited single phase SnS layers grown at 80 °C bath temperature fitted using Expo-2014 software. The good quality of fitting is represented by GOF (goodness of fit) of the Rietveld refinement, which is 1.482, indicating well resolved individual peaks. The refinement analysis shows orthorhombic crystal structure to the SnS layers, shown in the inset of Fig. 5. The lattice parameters calculated using refinement software were a = 4.091 Å, b = 11.102 Å, c = 3.970 Å. The estimated values of expected R_p factor and the weighted profile (R_{WP}) factor are 5.780 and 7.635. Therefore, the crystalline structure of SnS did not alter by the surface modification.

3.1.2. Raman analysis

The Raman analysis was carried out for further phase con-

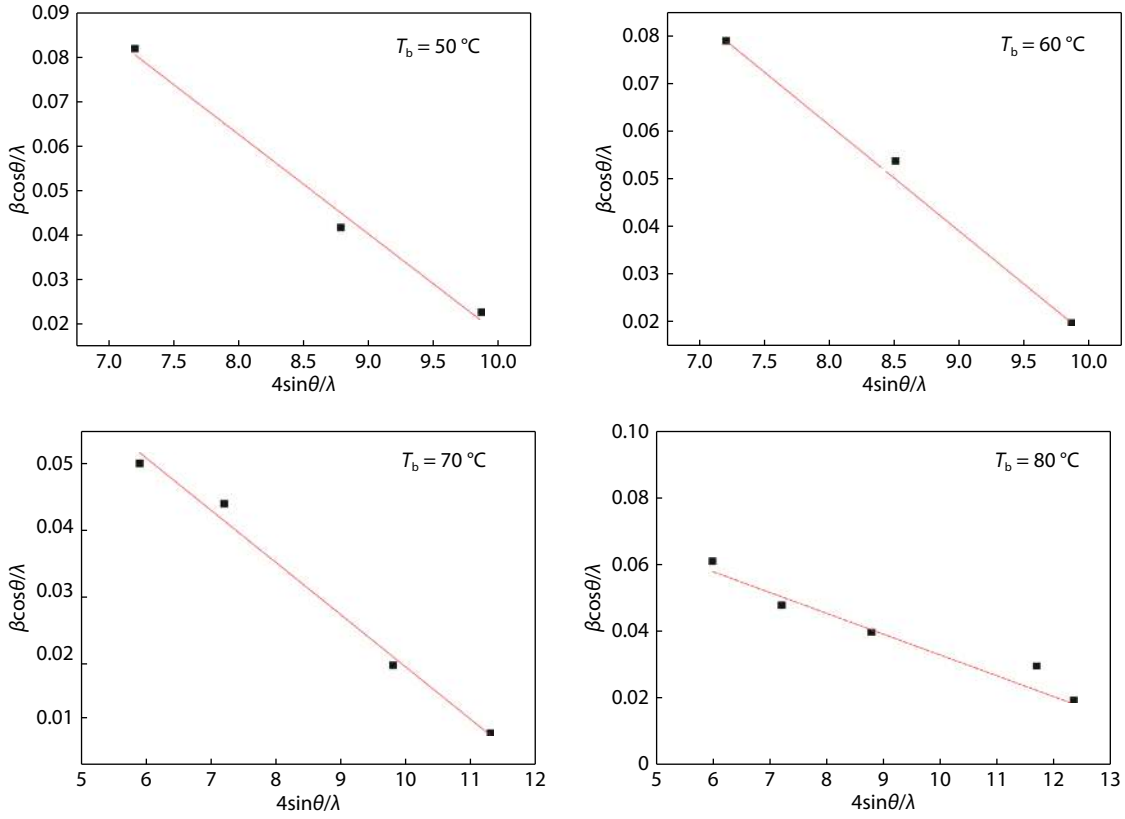

Fig. 5. (Color online) W-H plots of SnS layers with bath temperature.

Table 2. Structural parameters of PVA capped SnS layers formed at different bath temperatures with respect to (040) plane.

T_b (°C)	FWHM (°)	d_{XRD} (Å)	d_{JCPDS} (Å)	D (nm)		δ (10^{15} lines/m^2)	ε (10^{-3})		N (10^{15})
				Scherrer's formula	W-H plot		Scherrer's formula	W-H plot	
50	0.76048	2.828	2.835	11	4.0	7.8	11.8	22.4	62.4
60	0.72434	2.827	2.835	12	4.3	7.0	11.1	22.2	53.8
70	0.40719	2.825	2.835	21	10	2.2	6.1	7.8	9.7
80	0.38693	2.823	2.835	22	11	2.0	5.9	6.9	8.4

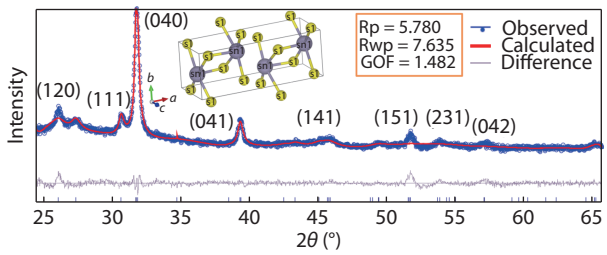

Fig. 6. (Color online) Rietveld refinement of SnS layers capped by PVA at 80 °C bath temperature.

firmation on the deposited layers as it is more sensitive to structural and compositional changes in the material. Fig. 4 shows the deconvoluted Raman spectra of the synthesized films deposited at different bath temperatures that varied in the range, 50–80 °C. At lower bath temperatures (< 70 °C), the spectra showed five characteristic peaks of tin monosulphide that appeared at 94, 166, 178, 219 and 225 cm^{-1}. In addition to these, other peaks related to Sn_2S_3 phase (307 cm^{-1}) and SnS_2 phase (312 cm^{-1}) were also observed. Films deposited at higher bath temperatures (≥ 70 °C) showed the Raman modes corresponding to tin monosulphide phase at 94, 166, 178 and 225 cm^{-1}. In general, SnS with orthorhombic crystal structure had 21 optical phonon modes. Among these modes, 12 are Raman active ($4A_g$, $2B_g$, $4B_{2g}$ and $2B_{3g}$), 7 are infrared active ($3B_{1u}$, $3B_{3u}$ and $1B_{2u}$), and 2 are inactive ($2A_u$)[60]. The observed Raman modes at 94, 219 and 225 cm^{-1} were assigned to A_g[52] whereas the mode present at 166 cm^{-1} was assigned to B_{3g}[61] and the mode at 178 cm^{-1} was assigned to B_{2g}[52]. The observed Raman modes are in good agreement with the reported data on SnS layers[52, 60–63]. This high intense Raman mode at 94 cm^{-1} peak is transverse optic (TO) mode that corresponds to the rigid shear modes of a layer with respect to its neighbours in the a, b directions[60].

In all the deposited layers, Raman mode appeared at 94 cm^{-1} had the highest intensity compared to other modes. A similar trend of Raman spectra with 94 cm^{-1} as an intense peak was observed by Sall *et al.*[52] in SnS films prepared by chemical spray pyrolysis. Arulantham *et al.*[63] also observed a strong Raman mode at 94 cm^{-1} in SnS thin films prepared by nebulizer spray pyrolysis technique. Further, the relative intensity of Sn_2S_3 and SnS_2 peaks decrease with the increase of bath temperature from 50 to 80 °C whereas the intensity of SnS peaks increases gradually. Thus the layers formed at higher bath tem-

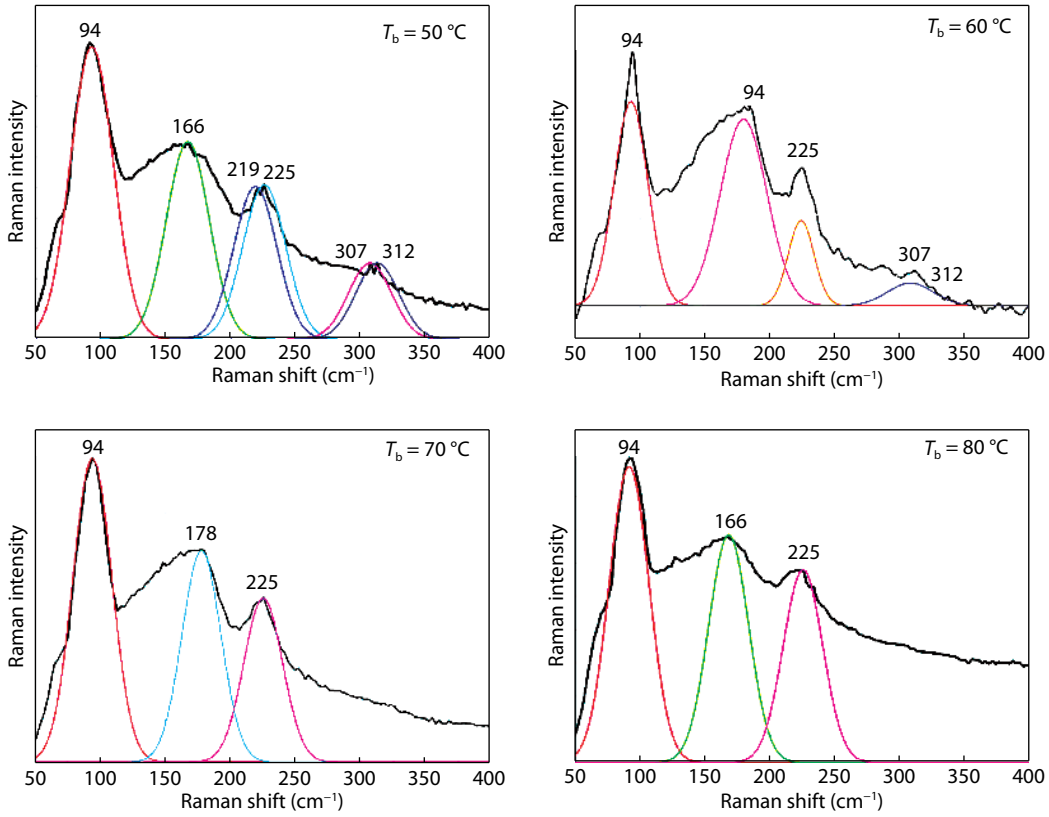

Fig. 7. (Color online) Deconvoluted Raman spectra of SnS layers grown at different bath temperatures.

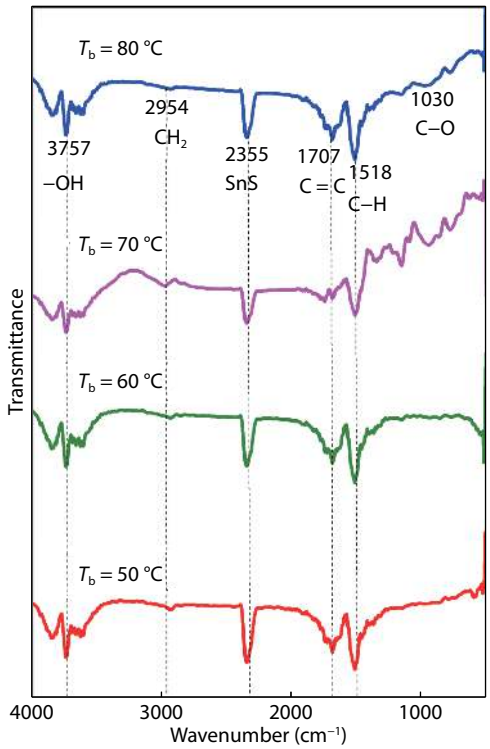

Fig. 8. (Color online) FTIR pectra of SnS layers grown at different bath temperatures.

peratures (⩾ 70 °C) had shown pure SnS phase without any secondary phases, supporting the XRD observations. Moreover, the intensity of Raman peaks increases with the increase of bath temperature, which might be due to an improvement in the crystallinity of the layers as noted in the XRD spectra.

3.2. FTIR analysis

The Fourier transform infrared spectral measurements were made for further confirmation of the interaction between PVA and SnS nanocrystals by identifying the absorbed functional groups on the crystallite surface of the grown layers. Fig. 8 shows the FTIR transmission mode spectra of the deposited PVA capped SnS layers deposited at different bath temperatures that varied in the range, 50–80 °C. The spectra showed characteristic bands of O–H, CH_2, C–H, C=C and C–O groups. The characteristic band at 3757 cm^{-1} is due to O–H stretching vibration of hydroxyl groups of PVA. The band at 2938 cm^{-1} corresponds to CH_2 asymmetric stretching vibration. The band at 1707 cm^{-1} is attributed to C = C stretching vibration. The band at 1518 cm^{-1} is generally ascribed to C–H bending vibration and the band at 1030 cm^{-1} assigned to C–O stretching of acetyl groups present in PVA. From these characteristic bands, it is confirmed the presence of PVA used in the synthesis of experimental SnS layers. In addition to these bands, the spectra showed a strong band at 2355 cm^{-1}, which represents the characteristic band of SnS[64] confirming its presence in the layers.

3.3. Surface morphology and topography

3.3.1. Morphological studies

Fig. 9 shows the SEM micrographs of SnS thin films capped by PVA grown at different bath temperatures varying from 50 to 80 °C. The morphology of SnS layers deposited at higher bath temperatures is different from those synthesized at lower bath temperatures. Layers formed at a bath temperature of 50 °C had a sponge-like structure of SnS nanocrystals and the layers deposited at 60 °C had an uneven distribution of grains due to the presence of voids. Large size and closely packed spherical shaped crystals were noticed in the films

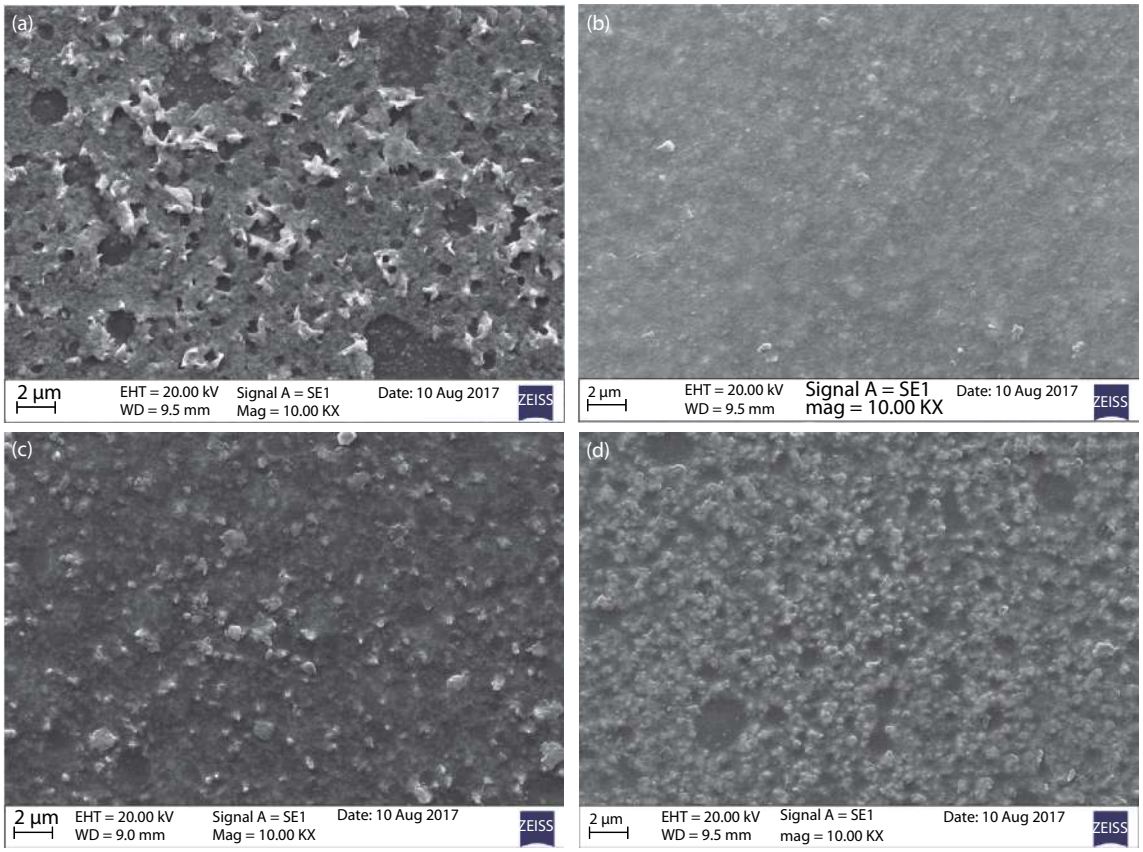

Fig. 9. (Color online) SEM images of SnS layers grown at different bath temperatures (a) 50 °C, (b) 60 °C , (c) 70 °C, and (d) 80 °C.

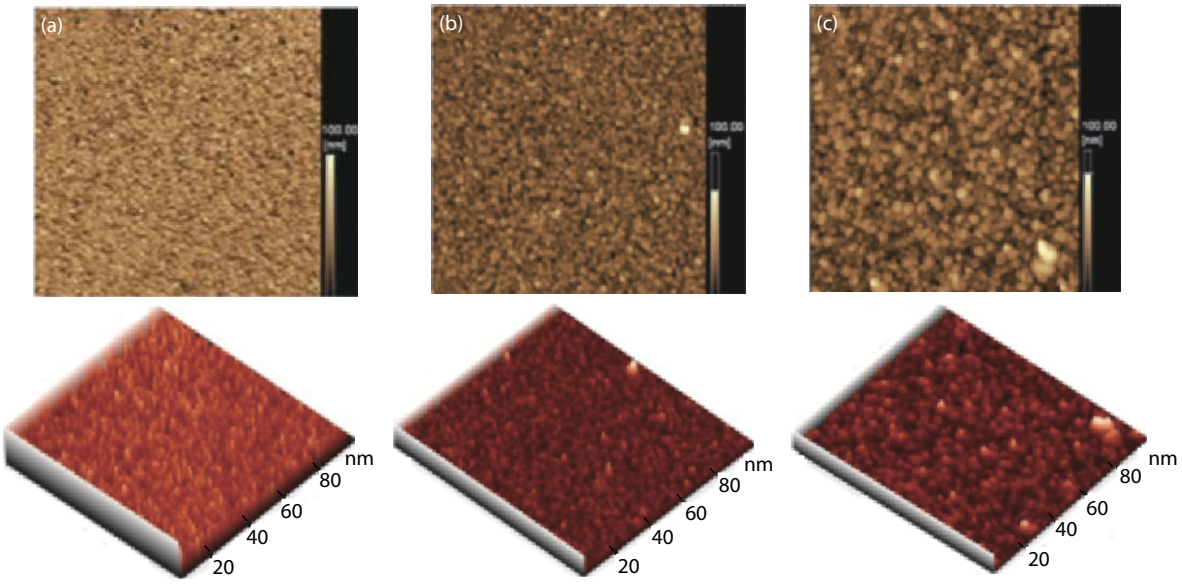

Fig. 10. (Color online) 2D and 3D AFM micrographs of SnS layers formed at different bath temperatures (a) 60 °C, (b) 70 °C, and (c) 80 °C.

formed at 70 and 80 °C bath temperatures. This is because of an improvement in the crystallinity of the layers formed at higher temperatures due to secondary nucleation. In fact at higher temperatures, the bonds between -OH group and the nanocrystals became weak and hence an interaction occurs between more number of particles, which leads to an increase in the size of the particles[65]. This result is in consistent with XRD and Raman observations.

3.3.2. Topographical analysis

AFM analysis was carried out to study the surface topography of PVA capped SnS layers. Fig. 10 shows the 2-dimensional AFM images along with 3D images of the prepared SnS films. AFM studies shows the gradual change in surface roughness and morphology of the experimental films with varied bath temperature. The average surface roughness of SnS films capped by PVA was evaluated using the AFM data that varied in the range, 2.6–3.2 nm, where the films formed at lower temperatures had slightly higher roughness and vice versa. It is also observed from the topographical analysis that the particles grew in irregular shape with a smaller size at lower

Table 3. Atomic weight (at.%) composition determined using EDS at different bath temperatures.

Bath temperature (°C)	Sn (at.%)	S (at.%)	Sn/S
50	30.24	65.50	0.46
60	36.36	60.66	0.59
70	46.15	51.53	0.89
80	48.26	50.28	0.95

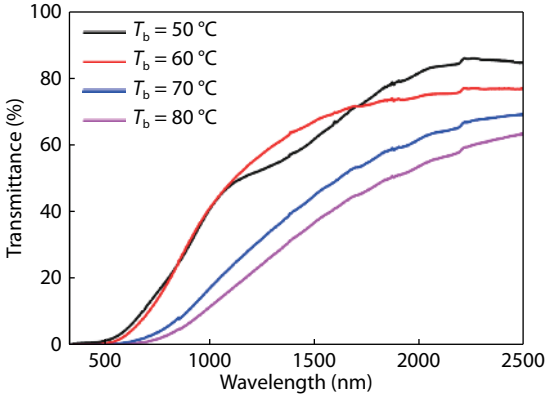

Fig. 11. (Color online) Variation of optical transmittance as a function wavelength in SnS films.

bath temperatures (< 70 °C). This is mainly due to insufficient thermal energy for the atoms and hence they could not move over the surface to form larger crystallites. However, at higher bath temperatures (⩾ 70 °C), there is an improvement in the particle size due to secondary nucleation and the layers exhibited spherically shaped grains. This behaviour was already observed in the XRD, Raman and SEM studies. The observed average particle size obtained by AFM analysis increased from 4.9 to 7.6 nm with bath temperature.

3.4. Compositional analysis

The elemental compositions of the PVA capped SnS thin films as a function of bath temperature was studied using EDS technique. Table 3 shows the compositions of Sn and S elements present in the films prepared at various bath temperatures. The analysis showed the presence of Sn and S elements in the deposited films. With the increase of bath temperature from 50 to 80 °C, the Sn/S ratio of SnS films grown in this work varied in the range, 0.46–0.95. At lower bath temperatures (T_b ⩽ 60 °C), the films showed sulfur rich composition, which indicates a less reaction of sulfur with Sn source in the reaction bath. As the bath temperature was increased to 70 °C and above, the composition ratio of Sn and S was increased from 0.89 to 0.95. This is because of an enhancement of reaction rate at higher bath temperatures. Films prepared at T_b = 80 °C showed the film composition close to stoichiometry (Sn/S ratio of approximately 1.0), which indicates the successful reaction in the bath.

3.5. Optical studies

The optical transmittance spectra of PVA capped SnS layers grown at different bath temperatures as a function of wavelength recorded in the range, 300–2500 nm is shown in Fig. 11. The spectra showed a decrease in optical transmittance with the increase of bath temperature, which indicates high absorbance in the layers formed at higher bath temperatures. Therefore, the absorption edge was shifted towards the

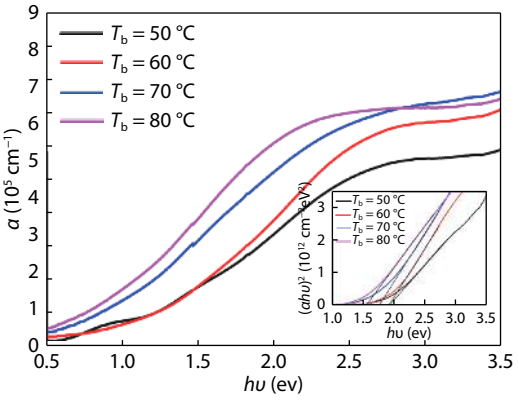

Fig. 12. (Color online) Change of absorption coefficient as a function of photon energy in the SnS films. (Inset) Tauc plots of SnS films.

Table 4. Comparison of particle size of SnS nanocrystals capped by PVA estimated using XRD, AFM and optical measurements.

T_b (°C)	Particle size from XRD analysis (nm)	Particle size from AFM micrographs analysis (nm)	Particle size from optical measurements (nm)
50	4.0	–	5.1
60	4.3	4.9	5.3
70	10	5.3	6.1
80	11	7.6	8.4

red region with the increase of bath temperature. The optical absorption coefficient (α) in the absorption region was determined using the formula[47],

$$\alpha = \frac{-\ln(T)}{t}, \tag{7}$$

where T is the transmittance and t is the thickness of the film.

The evaluated value of absorption coefficient for all layers was ~ 10^5 cm^{-1}, indicating that the films were highly absorbing and therefore they may be useful as an absorber layer for photovoltaic device fabrication. A plot of absorption coefficient (α) versus $h\upsilon$ for deposited films formed at different bath temperatures is shown in Fig. 12. It is evident from the plot that the absorption coefficient directly varies with temperature and hence the layers formed at 80 °C has maximum absorption coefficient. The energy band gap of the films is calculated using the expression[66],

$$\alpha h\upsilon = A(h\upsilon - E_g)^{1/2}, \tag{8}$$

where A is constant and $h\upsilon$ is photon energy. The Tauc plots of $(\alpha h\upsilon)^2$ versus $h\upsilon$ for the layers deposited at different bath temperatures are shown in the inset of Fig. 12. By extrapolating the linear portion of the curve onto the energy axis, the energy band gap was determined and an enhancement in the energy band gap has been observed for all the grown layers. The calculated energy band gap values for layers deposited decreased from 1.92 to 1.55 eV with the increase of bath temperature, which are higher than that of bulk value of SnS (1.3 eV). The observed blue shift in energy band gap values for the films deposited at bath temperatures (< 70 °C) is due to the presence of secondary phases that had higher energy band gaps. Whereas for the films deposited at bath temperatures (⩾ 70 °C), the observed increase in band gap is attributed

to the quantum confinement effect. A similar behaviour is also noted in the literature by Jana *et al.*[14] in PbS/PVA nanocrystals, Ojha *et al.*[67] in ZnS/PVA nanoparticles and also by Elashmawi *et al.*[45] in CdS/PVA nanorods.

Using energy band gap values, the average particle size at a particular growth temperature can be estimated using Brus equation[68],

$$E_{\mathrm{n}} = E_{\mathrm{g}} + \frac{h^2}{8R^2}\left[\frac{1}{m_{\mathrm{e}}{}^*} + \frac{1}{m_{\mathrm{h}}{}^*}\right] - \frac{1.8e^2}{\varepsilon R}\,(\mathrm{eV}), \qquad (9)$$

where E_{n} is the energy band gap of deposited SnS films, E_{g} is the energy band gap of bulk SnS, $m_{\mathrm{e}}{}^*$ is the effective mass of excited electron, $m_{\mathrm{h}}{}^*$ is the effective mass of excited hole, h is the Plank's constant, e is the charge of an electron, ε is the dielectric constant of SnS and R is the radius of the nanoparticle. In the present investigation, the different values are taken as E_{g} = 1.3 eV, $m_{\mathrm{e}}{}^* = 0.5m_0$, $m_{\mathrm{h}}{}^* = 0.109m_0$[31] and ε = 12.4[69]. The particle size determined by using Eq. (8) for films formed at different bath temperatures varied in the range 5.1–8.4 nm, where the particle size increases with the increase of bath temperature. The particle size evaluated from XRD, AFM and optical measurements are compared and given in Table 4.

4. Conclusions

Tin monosulphide thin films have been successfully grown using PVA as the capping agent for the first time by chemical bath deposition technique. The layers were formed on glass substrates at different bath temperatures that varied in the range, 50–80 °C. XRD studies revealed that all the deposited films had (040) peak as the preferred orientation that corresponds to SnS. Layers formed at lower bath temperatures, < 70 °C showed secondary phases of Sn_2S_3 and SnS_2, which disappeared when the temperature was increased to 70 °C. The Raman spectra supported this behaviour and showed relevant modes of different phases observed at different temperatures. XRD and Raman studies indicated an increase in crystallite size with increase of bath temperature. FTIR spectra clearly proved that the deposited SnS layers were capped by PVA. SEM analysis exhibited an increase of grain size with bath temperature whereas AFM studies indicated a decrease in surface roughness and an increase in particle size with the increase of bath temperature. The optical studies showed a direct optical absorption in the films. Optical band gap enhancement has been observed, where the energy band gap decreased from 1.92 to 1.55 eV with the increase of bath temperature. The single phase nanocrystalline PVA capped SnS layers may find application in the development of photovoltaic devices.

References

[1] Kana A T, Hibbert T G, Mahon M F, et al. Organotin unsymmetric dithiocarbamates: Synthesis, formation and characterization of tin (II) sulphide films by atmospheric pressure chemical vapour deposition. Polyhedron, 2001, 20, 2989

[2] Reddy K T R, Reddy N K, Miles R W, et al. Photovoltaic properties of SnS based solar cells. Sol Energy Mater Sol Cells, 2006, 90, 3041

[3] Guneri E, Gode F, Ultas C, et al. Effect of deposition time on structural, electrical, optical properties of SnS thin films deposited by chemical bath deposition. App Surf Sci, 2010, 257, 1189

[4] Reddy N K, Reddy K T R. Optical behaviour of sprayed tin sulphide thin films. Mater Res Bull, 2006, 41, 414

[5] Kawano Y, Chantana J, Minemoto T, et al. Impact of growth temperature on the properties of SnS films prepared by thermal evaporation and its photovoltaic performance. Curr Appl Phys, 2015, 15, 897

[6] Ganchev M, Vitanvov P, Sendova-Vassileva M, et al. Properties of SnS thin films grown by physical vapour deposition. J Phys: Conf Ser, 2016, 682, 012019

[7] Cheng S, Chen Y, He Y, et al. The structure and properties of SnS thin films prepared by pulse electro deposition. Mater Lett, 2007, 61, 1408

[8] El-Nahass M M, Zeyada H M, Aziz M S, et al. Optical properties of thermally evaporated SnS thin films. Opt Mater, 2002, 20, 159

[9] Andrade-Arvizu J A, Garcia-Sanchez M F, Courel-Piedrahita M, et al. Suited growth parameters including type of conductivity conversions on chemical spray pyrolysis synthesized SnS thin films. J Anal Appl Pyrolysis, 2016, 121, 347

[10] Haraa K O, Suzuki S, Usami N, et al. Formation of metastable cubic phase in SnS thin films fabricated by thermal evaporation. Thin Solid Films, 2017, 639, 7

[11] Tanusevski A, Poelman D. Optical and photoconductive properties of SnS thin films prepared by electron beam evaporation. Sol Energy Mater Sol Cells, 2003, 80, 297

[12] Ana V, Dronova M, Zakharov A, et al. Optical and AFM studies on p-SnS films deposited by magnetron sputtering. Chalcogenide Lett, 2015, 12, 483

[13] Banu S, Ahn S J, Eo Y J, et al. Thin monosulphide (SnS) thin films grown by liquid-phase deposition. Solar Energy, 2017, 145, 33

[14] Jana S, Thapa R, Maity R, et al. Optical and dielectric properties of PVA capped nanocrystalline PbS thin films synthesized by chemical bath depostition. Physica E, 2008, 40, 3121

[15] Subramaniam E P, Rajesh G, Muthukumarasamy N, et al. Solar cells of Cu_2ZnSnS_4 thin films prepared by chemical bath deposition method. Indian J Pure Ap Phy, 2014, 52, 620

[16] Jing J, Cao M, Wu C, et al. Chemical bath deposition of SnS nanosheet thin films for FTO/SnS/CdS/Pt photocathode. J Alloys Compd, 2017, 726, 720

[17] Chalapathi U, Poornaprakash B, Park S H, et al. Chemically deposited cubic SnS thin films for solar cell applications. Solar Energy, 2016, 139, 238

[18] Chaki S H, Chaudhary M D, Deshpande M P. SnS thin films deposited by chemical bath deposition, dip coating and SILAR. J Semicond, 2016, 37, 053001

[19] Nair M T S, Nair P K. Simplified chemical bath deposition for good quality SnS thin films. Semicond Sci Technol, 1991, 6, 132

[20] Nair P K, Nair M T S, Garcia V M, et al. Semiconductor thin films by chemical bath deposition for solar energy related applications. Sol Energy Mater Sol Cells, 1998, 52, 313

[21] Reighima M, Akkari A, Guasch C, Kamoun N T, et al. Synthesis and characterization of Fe-doped SnS thin films by chemical bath deposition technique for solar cell applications. J Renew Sustain Energy, 2013, 5, 063109

[22] Kumar K S, Manoharan C, Dhanapandian S, et al. Effect of Sb dopant on the structural, optical and electrical properties of SnS thin films by spray pyrolysis technique. Spectrochimica Acta A, 2013, 115, 840

[23] Chaki S H, Chaudhary M D, Deshpande M P, et al. Effect of indium and antimony doping in SnS single crystal. Mater Res Bull, 2015, 63, 173

[24] Kafasham H, Ebrahimi-Kahrizsangi R, Jamali-Sheini F, et al. Effect of Al doping on the structural and optical properties of electrodeposited SnS thin films. Phys Status Solidi A, 2016, 5, 1302

[25] Deepa K G, Nagaraju J. Growth and photovoltaic performance of SnS quantum dots. Mater Sci Eng B, 2012, 177, 1023

[26] Alam F, Dutta V. Tin sulphide (SnS) nanostructured films deposited by continuous spray pyrolysis (CoSP) technique for dye-sensitized solar cell applications. Appl Surf Sci, 2015, 358, 491

[27] Park J, Hwang C H, Young Lee W, et al. Preparation of size tunable SnS nanoparticles by a sonochemical method under multi-bubble sonoluminescence conditions. Mater Lett, 2014, 117, 188

[28] Azizian-Kalandaragh Y, Khodayari A, Zeng Z, et al. Strong

quantum confinement effects in SnS nanocrystals produced by ultrasound-assisted method. J Nanoparticle Res, 2013, 15, 1388
[29] Babu P, Reddy M V, Sreedevi G, et al. Status review on earth-abundant and environmentally green Sn–X (X = Se, S) nanoparticle synthesis by solution methods for photovoltaic applications. Int J Hydrog Energy, 2017, 42, 2790
[30] Bala V, Sharma M, Tripathi S K, et al. Investigations of AI: CdS/PVA nanocomposites: A joint theoretical and experimental approach. Mater Chem Phys, 2014, 146, 523
[31] Ramrakhiani M, Nogriya V. Photo and electro-luminescence of cadmium selenide nanocrystals and nanocomposites. J Lumin, 2013, 133, 129
[32] Hmar J J L, Majumder T, Mondal S P, et al. Growth and characteristics of PbS/polyvinyl alcohol nanocomposites for flexible high dielectric thin film applications. Thin Solid Films, 2016, 598, 243
[33] Elashmawi I S, Abdelghany A M, Hakeema N A, et al. Quantum confinement effects of CdS nanoparticles dispersed within PVP/PVA nanocomposites. J Mater Sci Mater Electron, 2014, 24, 2956
[34] Begum S K M, Nirmala G, Ravindranadh K, et al. Physical and spectral investigations of Mn^{2+} ions doped poly vinyl alcohol capped ZnSe nanoparticles. J Mol Struct, 2011, 1006, 344
[35] Zakaria A, Zamiri R, Vaziri P, et al. Thermal diffusivity measurement of cadmium sulphide nanoparticles prepared by γ-radiation technique. Int J Phys Math Sci, 2011, 5, 928
[36] Sagitha P, Sarada K, Muralidharan K, et al. One pot synthesis of poly vinyl alcohol (PVA) supported silver nanoparticles and its efficiency in catalytic reduction of methylene blue. Trans Nonferrous Met Soc China, 2016, 26, 2693
[37] Murugadoss G, Rajesh kumar M. Synthesis and optical properties of monodispersed Ni^{2+} doped ZnS nanopaarticles. Appl Nanosci, 2014, 4, 67
[38] Osuntokun J, Ajibade P A. Morphology and thermal studies of zinc sulphide and cadmium sulphide nanoparticles in polyvinyl alcohol matrix. Physica B, 2016, 496, 106
[39] Mohamed S A, AI-Ghamdi A A, Sharma G D, et al. Effect of ethylene carbonate as a plasticizer on CuI/PVA nanocomposite: Structure, optical and electrical properties. J Adv Res, 2014, 5, 79
[40] Seoudi R, EI Mongy S A, Shabaka A A, et al. Effect of polyvinyl alocohol matrices on the structural and spectroscopic studies of CdSe nanoparticles. Physica B, 2008, 403, 1781
[41] Sharma M, Tripathi S K. Optical and electrical properties of polyvinyl alcohol doped CdS nanoparticles prepared by sol–gel method. J Mater Sci Mater Electron, 2015, 26, 2760
[42] Elashmawi I S, Hakeema N A, Soliman Selim M, et al. Optimization and spectroscopic studies of CdS/polyvinyl alcohol nanocomposites. Mater Chem Phys, 2009, 115, 132
[43] Tamgadge Y S, Sunatkari A L , S, Talwatkar S, et al. Linear and nonlinear optical properties of nanostructured $Zn_{(1-x)}Sr_xO$-PVA composite thin films. Opt Mater, 2014, 37, 42
[44] Singh N, Mehra R M, Kapoor A. ZnO based quantum dot sensitized solar cell using CdS quantum dots. J Renew Sustain Energy, 2012, 4, 013110
[45] Phukan P, Saikia D. Optical and structural investigation of CdSe quantum dots dispersed in PVA matrix and photovoltaic applications. Int J Photoenergy, 2013, 2013, 728280
[46] Saikia D, Phukan P. Fabrication and evaluation of CdS/PbS thin film solar cell by chemical bath deposition technique. Thin Solid Films, 2014, 562, 239
[47] Sreedevi G, Reddy M V, Park C, et al. Comprehensive optical studies on SnS layers synthesized by chemical bath deposition. Opt Mater, 2015, 42, 468
[48] Reddy V R M, Sreedevi G, Park C, et al. Development of sulphurized SnS thin film solar cells. Curr Appl Phys, 2015, 15, 588
[49] Nwankwo S N, Campbell S, Reddy K T R, et al. Temperature controlled properties of sub-micron thin SnS films. Semicond Sci Technol, 2018, 33, 065002
[50] Hwang D H, Shin J Y, Lee S, et al. Substrate temperature effects on the properties of radio-frequency sputtered SnS thin films. Nanosci Nanotechnol Lett, 2018, 10, 696
[51] Clayton A J, Charbonneau C M E, Tsoi W C, et al. One-step growth of thin film SnS with large grains using MOCVD. Sci Technol Adv Mater, 2018, 19, 153
[52] Sall T, Soucase B M, Mollar M, et al. SnS thin films prepared by chemical spray pyrolysis at different substrate temperatures for photovoltaic applications. J Electron Mater, 2017, 46, 1714
[53] Assilli K, Alouani K, Vilanova X. Impact of deposition temperature on the properties of SnS thin films grown over silicon substrate-comparative study of structural and optical properties with films grown on glass substrates. Semicond Sci Technol, 2017, 32, 115005
[54] Al Shakban M, Xie Z, Savjani N, et al. A facile method for the production of SnS thin films from melt reactions. J Mater Sci, 2016, 51, 6166
[55] Saenk N S. The X-ray diffraction study of three-dimensional disordered network of nanographites: experiment and theory. Physics Procedia, 2012, 23, 102
[56] Purohit A, Chander S, Nehra S P, et al. Effect of air annealing on structural, optical, morphological and electrical properties of thermally evaporated CdSe thin films. Physica E, 2015, 69, 342
[57] Sarmah K, Sarma R, Das H L. Structural characterization of thermally evaporated CdSe thin films. Chalcogenide Lett, 2008, 5, 153
[58] Jassim S A J, Ali Zumaila A A R, et al. Influence of substrate temperature on the structural, optical and electrical properties of CdS thin films deposited by thermal evaporation. Results in Physics, 2013, 3, 173
[59] Prabhu Y T, Rao K V, Kumar V S S, et al. X-ray analysis by Williamson-Hall and size-strain methods of ZnO nanoparticles with fuel variation. World J Nano Sci Eng, 2014, 4, 21
[60] Baby B H, Vaisakh V M, Mohan D B, et al. Fabrication and phase characterization study of SnS thin films under controlled sulfur deposition temperature. Mater Today, 2016, 3, 2077
[61] Ali S, Wang F, Zafar S, et al. Characterization and Raman vibrations of chalcogenide SnS nanorods. IOP Conference Series: Materials Science and Engineering, 2017, 275, 012007
[62] Jayasree Y, Chalapathi U, Bhaskar P U, et al. Effect of precursor concentration and bath temperature on the growth of chemical bath deposited tin sulphide thin films. Appl Surf Sci, 2012, 258, 2732
[63] Arulanantham A M S, Valanarasu S, Jeyadheepan K, et al. Development of SnS (FTO/CdS/SnS) thin films by nebulizer spray pyrolysis (NSP) for solar cell applications. J Mol Struct, 2018, 1152, 137
[64] Das D, Dutta R K. A novel method of synthesis of small band gap SnS nanorods and its efficient photocatalytic dye degradation. J Colloid Interface Sci, 2015, 457, 339
[65] Onwudiwe D C, Kruger T P J, Oluwatobi O S, et al. Nanosecond laser irradiation synthesis of CdS nanoparticles in a PVA system. Appl Surf Sci, 2014, 290, 18
[66] Guddeti P R, Gedi S, Reddy K T R, et al. Sulfurization temperature dependent physical properties of Cu_2SnS_3 films grown by a two-stage process. Mater Sci Semicond Process, 2018, 86, 164
[67] Ojha K S. Structural and optical properties of PVA doped zinc sulphide thin films. Optik, 2016, 127, 2586
[68] Brus L. Electronic wave functions in semiconductor clusters: experiment and theory. J Phys Chem, 1986, 90, 2555
[69] Xu J, Yang Y. Study on the performances of SnS heterojunctions by numerical analysis. Energy Convers Manag, 2014, 78, 260